Information of the Journal in which the present paper is published:

- Royal Society of Chemistry. Molecular Biosystems 2015, (12):3397-406.
- doi: 10.1039/c5mb00413f.

# Epithelial-to-mesenchymal transition involves triacylglycerol accumulation in DU145 prostate cancer cells

Received 00th January 20xx,
Accepted 00th January 20xx

DOI: 10.1039/x0xx00000x

www.rsc.org/

Núria Dalmau[a], Joaquim Jaumot[a], Romà Tauler[a] and Carmen Bedia[a]

Epithelial to mesenchymal transition (EMT) is a biological process that plays a crucial role in cancer metastasis. Although studies regarding the EMT mechanisms are usual in terms of gene expression and protein functions, little is known about the involvement of lipids in EMT. In this work, an untargeted lipidomic analysis was performed to reveal which lipids are involved in the EMT process. DU145 prostate cancer cells were treated with TNFα, a well-known EMT inducer. After 6 hours of treatment, a decrease of cell membrane E-cadherin as well as a reduction in its gene expression were observed. Also, the mesenchymal markers Vimentin and Snail were up-regulated, suggesting that EMT started below 6 hours of treatment. Lipid extracts of untreated and TNFα-treated cells at short times were analyzed using ultra-performance liquid chromatography coupled to high-resolution mass spectrometry (UPLC-MS). Multivariate data analysis methods were applied to decipher which lipids presented significant changes after EMT induction. Among the results obtained, a significant increase of twelve unsaturated triacylglycerides (TAGs) was observed. This increase of TAGs was also observed for cells treated with TGFβ (another EMT inducer), suggesting that this feature is a common mechanism in the EMT process. In conclusion, this work reported for the first time a TAG accumulation through EMT induction. These TAG lipids could have a key role in providing cells with the energy, cell membrane components and signaling lipids necessary to guarantee the enhanced cell migration and proliferation of metastatic cells.

## Introduction

Epithelial-to-mesenchymal transition (EMT) is an essential process involved in multiple biological tasks such as tissue repair, wound healing and embryonic development. During EMT, epithelial cells lose their intercellular adhesion and apical-basal polarization, leading to an increase in their migratory and invasive properties [1, 2]. In cancer cells, this transition to a mesenchymal phenotype has been shown to be involved in tumour invasion and metastasis [3, 4]. EMT is characterized by the loss of epithelial markers such as membrane E-cadherin and β-catenin and the up-regulation of the transcription factors Snail, Twist, Slug and ZEB1 as well as mesenchymal markers such as vimentin and fibronectin [5].

Many cytokines and growth factors such as transforming growth factor beta (TGFβ), IL-6 and tumour necrosis factor alpha (TNFα) can induce EMT [6]. TNFα is a pro-inflammatory cytokine, involved in the regulation of multiple physiological and pathological processes including inflammation, immunity, cell proliferation and apoptosis. Increased TNFα expression levels have been associated with an increased grade malignancy and metastasis in prostate cancer [7]. This cytokine has been shown to induce EMT through activation of nuclear factor kappa beta (NF-κB), a transcription factor involved in cancer initiation and progression[8].

Lipids are a very diverse group of compounds with crucial roles in living organisms. Among their multiple biological functions, they contribute to cell compartmentalization, energy storage and production, cell signalling, protein trafficking, and

[a] Department of Environmental Chemistry, Institute of Environmental Assessment and Water Research (IDAEA-CSIC), c/ Jordi Girona 18-24, 08034 Barcelona, Spain

membrane organization. Despite the importance of lipids in cell homeostasis, little is known about the lipid composition of cells during EMT. Lipidomics is a branch of metabolomics consisting in the large-scale study of cellular lipids and their interaction with other lipids, proteins and metabolites [9]. It includes the comprehensive analysis of lipid species within a biological sample and the analysis of alterations in lipid content and composition after cell perturbation or pathogenesis [10]. These studies have been proved to be useful in the study of the mechanism of many diseases, as well as in the finding of specific disease biomarkers [11-13]. Two different analytical approaches exist in lipidomics: targeted and untargeted analyses. Whereas targeted lipidomic analyses are focused on the detection and quantitative analysis of some selected compounds, the aim of the untargeted analyses is to detect which lipid species show significant changes under specific stimuli, without any previous hypothesis of the lipids involved. The advantage of this approach is that it enables the discovery of unexpected lipid species associated with a certain biological process. This untargeted approach often involves the use of chemometric analysis methods on complex and massive amounts of data obtained in LC/GC-MS full scan analysis of samples.

In the present study, an untargeted lipidomic approach on EMT-induced prostate cancer cells under TNFα treatment was carried out. Data obtained from LC-MS on lipid extracts was further processed using chemometric analysis methods. The aim of this lipidomic research was to explore the changes in lipid composition in EMT-induced cells and to detect which lipid species are involved in the EMT process.

## Results

### TNFα induces EMT in DU145 cells

First of all, EMT induction was confirmed under TNFα exposure in DU145 prostate cancer cells. EMT was assessed by flow cytometry on cells exposed to TNFα (20 ng/ml) for 24 hours, using a specific antibody against E-cadherin, a characteristic epithelial cell marker. The results showed a reduction of the fluorescence associated to membrane E-cadherin (Fig. S1), indicating that the reported conditions induced EMT in DU145 cells.

Immunofluorescence images taken after 6 and 24 hours of TNFα treatment confirmed the loss of E-cadherin in cell membrane (Fig. 1a). Interestingly, 6 hours were sufficient to observe a decrease of E-cadherin green fluorescence. Also, formation of pseudopodia was found in plasma membranes after 6 hours of TNFα exposure. Pseudopodia are projections of cell membranes that involve changes in the cytoskeleton dynamics. Their formation has long been associated with tumour cell migration and invasion [14], and recently, to the acquisition of a motile and migratory phenotype in EMT [15]. According to this, qRT-PCR analysis further corroborated the EMT induction at early exposure times. As represented in Fig. 1b, TNFα significantly induced the down-regulation of E-cadherin at 5 and 6 hours. In addition, mRNA levels of the mesenchymal markers Vimentin and Snail increased significantly at 6 hours.

These observations suggested that changes leading to EMT under TNFα treatment occurred at early incubation times. According to this, the subsequent lipidomic study was performed at different exposure times below 6 hours.

### Lipidomic study of EMT

The lipidomic study was performed on cell cultures exposed to TNFα for 0, 3, 4, 5 and 6 hours (3 samples/each). Every sample was then subjected to two types of lipid extraction: 1) extraction using chloroform/methanol (2:1) that contains intact lipids from the sample; 2) extraction using chloroform/methanol (1:2) with a saponification step to remove all the ester lipids from the sample favouring the detection of sphingolipids. LC-MS profiles of lipid extractions and internal standards are available as Supplementary material (Fig S3-S6).

First, a preliminary study on total ion current (TIC) chromatograms, obtained in both positive and negative ionization modes was carried out by Partial Least Squares-Discriminant Analysis (PLS-DA). This classification study was performed on matrices containing the normalized TICs of

 

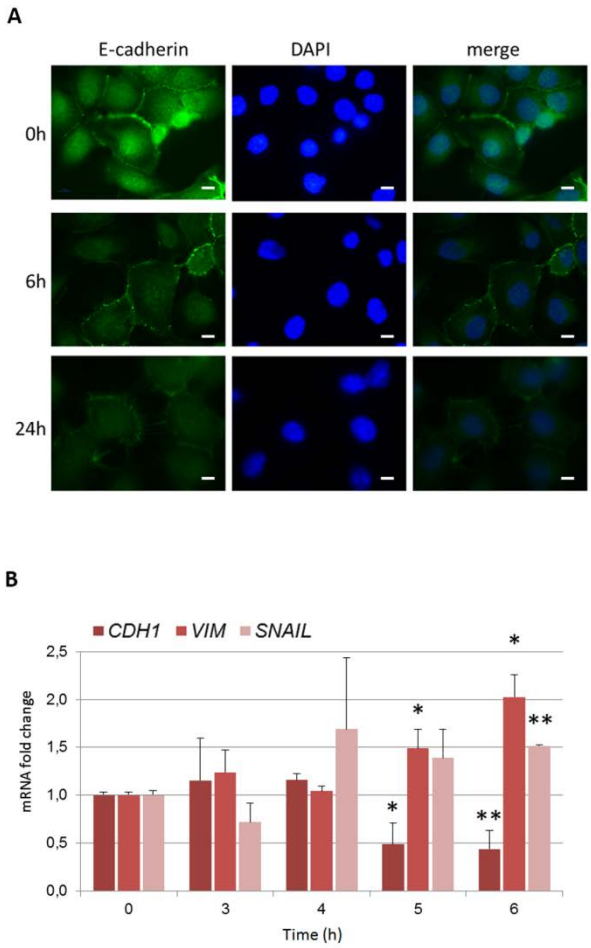


**Figure 1.** EMT induction in DU145 prostate cancer cells under TNFα treatment. A) Immunofluorescence assay on DU145 cells treated with TNFα (20 ng/ml) for 6 and 24 hours. After fixation, E-cadherin (green) was examined by green immunofluorescence staining with E-cadherin-FITC antibody. Nuclei were stained with DAPI (blue). Images are representative pictures of three independent experiments. Scale bars: 10 µm. B) Bar diagram of real-time quantitative PCR analysis of E-cadherin (CDH1), Vimentin (VIM) and Snail expression. Ct values were normalized to the Ct value of GAPDH from the same sample, and fold change expression was obtained using the delta-delta Ct method. Results represented the mean ± SE of three independent experiments (n=3) performed in triplicate. The indicated significant differences are considered respect to the untreated cells. * $p<0.05$, ** $p<0.01$

samples, in order to see if their lipidomic profiles could separate samples corresponding to different times of TNFα exposure. PLS-DA is a supervised classification analysis tool that requires prior knowledge of class membership. In this case, two classes were chosen and defined as pre-EMT and post-EMT: samples at 0 and 3 hours were grouped into the pre-EMT class and samples at 5 and 6 hours into the post-EMT class. These classes were defined considering that at 0 and 3 hours mRNA levels of the EMT markers were similar and significantly different to the expression levels observed at 5 and 6 hours. As a result, we observed a clear separation between pre-EMT and post-EMT samples in the positive mode (see Fig S2) suggesting that substantial changes in the lipidomic profile occurred as a consequence of the EMT induction under TNFα treatment. In contrast, the TICs of samples acquired in the negative mode in both extraction 1 and 2 could not be separated in the PLS-DA models, thus these data were not considered for further analysis.

In order to further investigate which specific lipids were altered during the EMT induction process, a deeper analysis of these data was carried out. Full scan LC-MS data matrices containing all intensity values measured at different mass and retention times in the positive ionization mode were analysed by means of Multivariate Curve Resolution - Alternating Least Squares (MCR-ALS). The mass values of the resolved peaks that presented significant changes between pre- and post-EMT samples were integrated using raw data files, and further normalized and identified as described in the methodology section. A new matrix containing the concentrations of the selected compounds in every sample (X-data) was constructed and subjected to a PLS-DA in order to confirm the discrimination between pre and post-EMT classes (y-data). Fig. 2 shows PLS-DA scores obtained in the analysis. For extraction 1 (intact lipids), 85.10% of Y-variance was explained by cumulative X-variance of 74.67% of two latent variables with a Matthews Correlation Coefficient (MCC) [16] equal to 0.7. In the case of extraction 2 (sphingolipids), 89.84% of Y-variance was explained by cumulative X-variance of 82.64% of three latent variables with a MCC of 0.8.

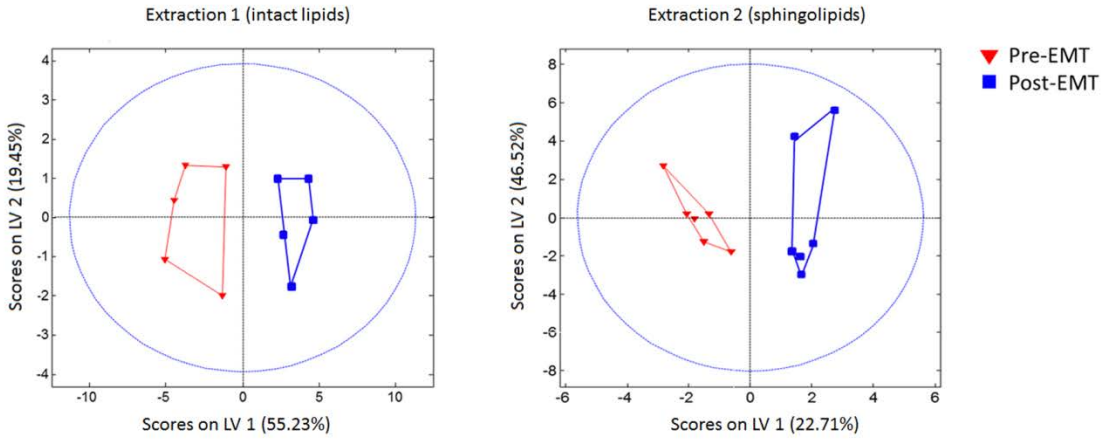


**Figure 2.** PLS-DA analysis of lipidomic data. Lipid extracts of DU145 cells treated with TNFα at different times were analysed through UPLC-TOF and data was imported into MATLAB environment. PLS-DA scores plots of matrices containing the concentrations of the selected compounds obtained by MCR-ALS analysis on full scan data matrices in the positive ionization mode.

These results indicated that specific lipid molecules whose profiles were resolved in the MCR-ALS analysis allowed the discrimination between pre-EMT and post-EMT samples. In the PLS-DA model obtained, the Variable Importance in Projection (VIP) scores [17] were calculated to investigate which were the most influent lipids in the discrimination of pre and post-EMT samples.

The complete detailed list of m/z values corresponding to the lipids that showed changes from 0-3 h to 5-6 h under TNFα treatment within both extraction 1 and 2 can be consulted in Table 1. This table, in which compounds are sorted by their chromatographic retention time, includes the annotation of lipids, performed as described in the experimental section. Only the listed lipids with a VIP score value greater than 1 and a mass error less than 10 ppm (blue highlighted rows) were selected for a further interpretation of lipidomic results.

The most relevant aspect of the results obtained was the increase of twelve different unsaturated triacylglycerides (TAGs) containing from 50 to 58 carbon atoms with fold-changes values ranging from 1.6 to 2.5. Also, a 1.4 fold increase was observed for phosphatidylcholine (40:5). Regarding sphingolipid species, an important decrease of ceramide 16:0 (Cer(16:0)) was detected (0.5 fold) with a VIP value of 2.2. Although Cer(16:0) is the only identified sphingolipid that presented substantial changes, its VIP value suggested that this reduction of ceramide is influencing sufficiently to allow the discrimination between pre- and post-EMT samples. This decrease is consistent with the results of Edmond et al.'s work [18], in which a down-regulation of CerS6 gene, responsible for the enzyme that synthesizes Cer(16:0), is reported in EMT.

**Confirmation of TAG enhancement in EMT induced DU145 cells**

To further explore the increase of TAG observed under TNFα treatment, the behaviour of all the TAGs listed in Table 1 was investigated. A time course was performed by exposing cells to TNFα (20 ng/ml) for 0, 6, 24 and 48 hours. Time course results showed a dependence of TAG increase over time under TNFα exposure. After 6 hours of treatment, TAG levels increased in similar proportions to that observed in the previous lipidomic study, reaching maximum levels at 24 hours. At 48 hours of

| ret. time | m/z measured | Identified Compound | adduct | m/z calculated | mass error (ppm) | pmol/mg protein in pre-EMT | pmol/mg protein in post-EMT | fold change | p value | VIP value | Database ID |
|---|---|---|---|---|---|---|---|---|---|---|---|
| **7.8** | 538.5208 | Cer (16:0) | M+H | 538.5194 | 2.60 | 194 ± 100 | 106 ± 18 | 0.5 | 0.0209 | 2.2 | HMBD04949 |
| **9.7** | 836.6181 | PC(40:5) | M+H | 836.6164 | 1.94 | 425 ± 83 | 581± 100 | 1.4 | 0.0362 | 1.0 | HMDB08218 |
| **16.1** | 846.7559 | TAG (50:3) | M+NH4 | 846.7545 | 1.64 | 326 ± 116 | 737± 228 | 2.2 | 0.0209 | 1.3 | HMDB47737 |
| **16.5** | 848.7717 | TAG(50:2) | M+NH4 | 848.7701 | 2.16 | 419 ± 137 | 866 ± 269 | 2.1 | 0.0209 | 1.2 | HMDB44034 |
| **16.5** | 922.7806 | TAG(56:7) | M+NH4 | 922.7858 | 5.22 | 305 ± 152 | 753 ± 167 | 2.5 | 0.0136 | 1.5 | HMDB45356 |
| **16.6** | 948.7969 | TAG(58:8) | M+NH4 | 948.8014 | 4.70 | 233 ± 111 | 582 ± 135 | 2.5 | 0.0136 | 1.6 | HMDB51044 |
| **16.7** | 874.787 | TAG(52:3) | M+NH4 | 874.7858 | 1.36 | 326 ± 104 | 724± 235 | 2.2 | 0.0136 | 1.3 | HMDB45489 |
| **16.9** | 950.8147 | TAG(58:7) | M+NH4 | 950.8171 | 2.22 | 241 ± 112 | 574 ± 123 | 2.3 | 0.0136 | 1.6 | HMDB50738 |
| **17.1** | 850.7863 | TAG(50:1) | M+NH4 | 850.7858 | 0.22 | 623 ± 114 | 1025 ± 269 | 1.6 | 0.0136 | 1.1 | HMBD45481 |
| **17.3** | 876.8036 | TAG(52:2) | M+NH4 | 876.8014 | 2.89 | 958 ± 229 | 1878 ± 467 | 2.0 | 0.0136 | 1.4 | HMDB42488 |
| **17.5** | 902.8262 | TAG(54:3) | M+NH4 | 902.8171 | 9.81 | 744 ± 195 | 1483 ± 392 | 2.0 | 0.0136 | 1.4 | HMBD46267 |
| **17.9** | 878.8126 | TAG(52:1) | M+NH4 | 878.8711 | 4.68 | 417 ± 90 | 628± 153 | 1.5 | 0.0362 | 0.9 | HMDB42453 |
| **17.9** | 916.8317 | TAG(55:3) | M+NH4 | 916.8328 | 1.16 | 186 ± 53 | 372 ± 87 | 2.0 | 0.0136 | 1.5 | HMDB43548 |
| **18.1** | 904.8357 | TAG(54:2) | M+NH4 | 904.8327 | 3.58 | 502 ± 116 | 882 ± 186 | 1.8 | 0.0136 | 1.4 | HMBD46436 |
| **18.6** | 956.8592 | TAG(58:4) | M+NH4 | 956.8640 | 5.29 | 140 ± 36 | 298 ± 71 | 2.1 | 0.0136 | 1.5 | HMDB46326 |

**Table 1.** Table list of the m/z values that presented significant changes (p-value <0.05) in their levels between pre-EMT and post-EMT group samples in both types of lipid extraction. The absolute concentrations of lipids were calculated considering the area of the corresponding internal standards added in the extraction (Cer, TAG and PC) and the protein content in each sample as follows: (200 x mg of protein)/area of specific standard. The assigned compound corresponds to the lipid molecule with the minimum mass error value respect to the measured m/z, considering all the possible adducts in the positive ionization mode. The list only contains the compounds with a Benjamini-Hochberg's corrected p-value <0.05. Blue highlighted rows indicate the lipids considered for further interpretation of results. Cer: ceramide; PC: phosphatidylcholine; TAG: triacylglyceride.

treatment, most of the TAGs still showed significantly enhanced levels (Fig. 3). This increase was also obtained by a MCR-ALS simultaneous analysis of 0 and 24 hours samples (data not shown), which confirmed the rise of TAGs levels. Also, we explored if the increase of TAG was accompanied by a rise of lipid droplets, which are lipid storage organelles consisting of a phospholipid monolayer that surrounds a core of neutral lipids, mainly TAGs and cholesterol esters. As depicted in Fig. 4a and 4b, lipid droplets, stained using Nile Red, were significantly increased in cells at 6 hours, with sustained elevated levels at 24 and 48 hours of TNFα treatment, confirming the lipid deposition of the newly synthesized TAG in these organelles. The increased levels of TAGs suggested an activation of lipogenic mechanisms. Thus, the expression of some lipogenic enzymes such as acetyl-CoA carboxylase α (ACACA) and fatty acid synthase (FASN) was investigated after 6 hours of TNFα exposure. As a result, whereas any significant change was observed for the expression of ACACA, FASN was found overexpressed (Fig. 4c). This observation suggested that FASN, which is responsible for the synthesis of new fatty acids and has been found to be highly expressed in prostate cancer [19], could be involved in the TAG accumulation observed.

To confirm that this rise of TAG was not a specific event of TNFα treatment, another widely known EMT inducer cytokine, transforming growth factor-beta (TGFβ) [20-22], was used. DU145 cells were treated with TGFβ (20ng/ml) for 0, 6, 24 and 48 hours. The induction of EMT was confirmed by the reduction of E-cadherin levels on cell membrane at 6 and 24 hours (see Fig 5a). Concerning the TAG species listed in Table 1, for most of them, TGFβ treatment induced a time-dependent rise in the levels of TAGs with significant fold increases for some of them at 24 hours (Fig. 5b), which was consistent with the

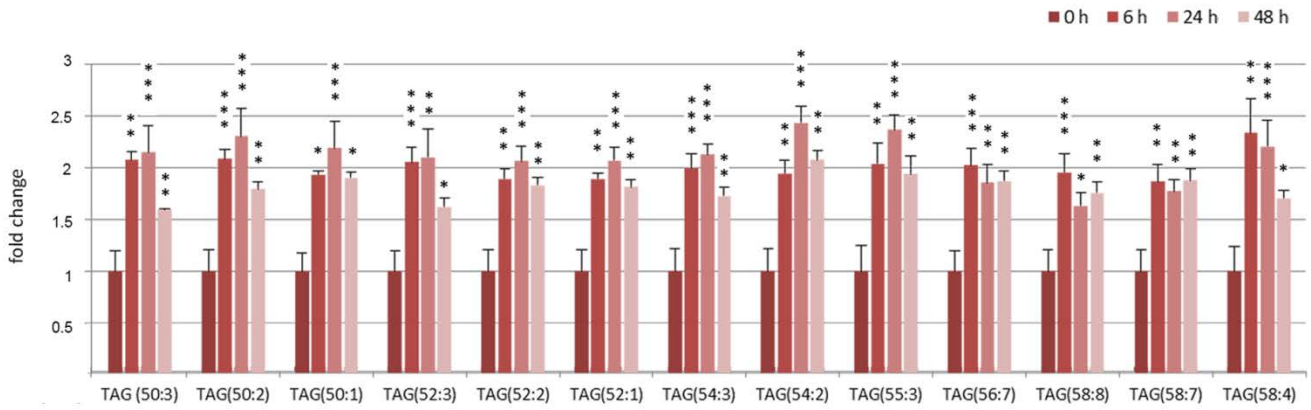


**Figure 3.** Time dependence of TAGs increase under TNFα treatment. A) DU145 cells were exposed to TNFα (20ng/ml) for 0, 6, 24 and 48 hours. Bar diagram of fold changes in the levels of the selected TAGs at the indicated times. Results are representative of two independent experiments performed in triplicate. The indicated significant differences are considered respect to the untreated cells. * p<0.05, ** p<0.01, *** p<0.005

observations obtained under TNFα treatment. In addition, we observed that lipid droplets also increased, with a maximum at 24 hours (Fig. 5c and 5d) Even though these results are not identical to those of TNFα, these similar features observed under both treatments suggested that TAGs has a relevant role in EMT.

## Discussion

Lipids contribute to several biological functions in cancer cells. First, they have a structural role in the production of cell membranes to support the high proliferation rate of cancer cells. Second, some of them such as diacylglycerol, sphingosine-1-phosphate or ceramide, act as second messengers in signalling transduction pathways controlling diverse cellular functions such as cell migration, proliferation or survival. Third, fatty acids (FAs) are able to induce post-translational modifications of proteins (i.e. palmitoylation) which control the function of various signalling processes [23]. Finally, FAs also can serve as a source of energy through β-oxidation to assure cancer cell survival.

Due to the essential functional roles of lipids in cancer cell maintenance and survival, we considered relevant the study of lipid changes involved in EMT, which constitutes a critical process involved in the transdifferentiation of epithelial cells into an invasive phenotype, a crucial mechanism that mediates cancer metastasis. In the context of EMT, few publications have reported changes in lipids during EMT. Guan et al. have shown that some specific glycosphingolipids (gangliotetraosylceramide and GM2) are reduced in an EMT process induced by TGFβ in mouse and human epithelial cell lines [24, 25]. In another recent article, CerS6 gene, responsible for Cer (16:0) synthesis, has showed to be down-regulated in EMT induced cells [18].

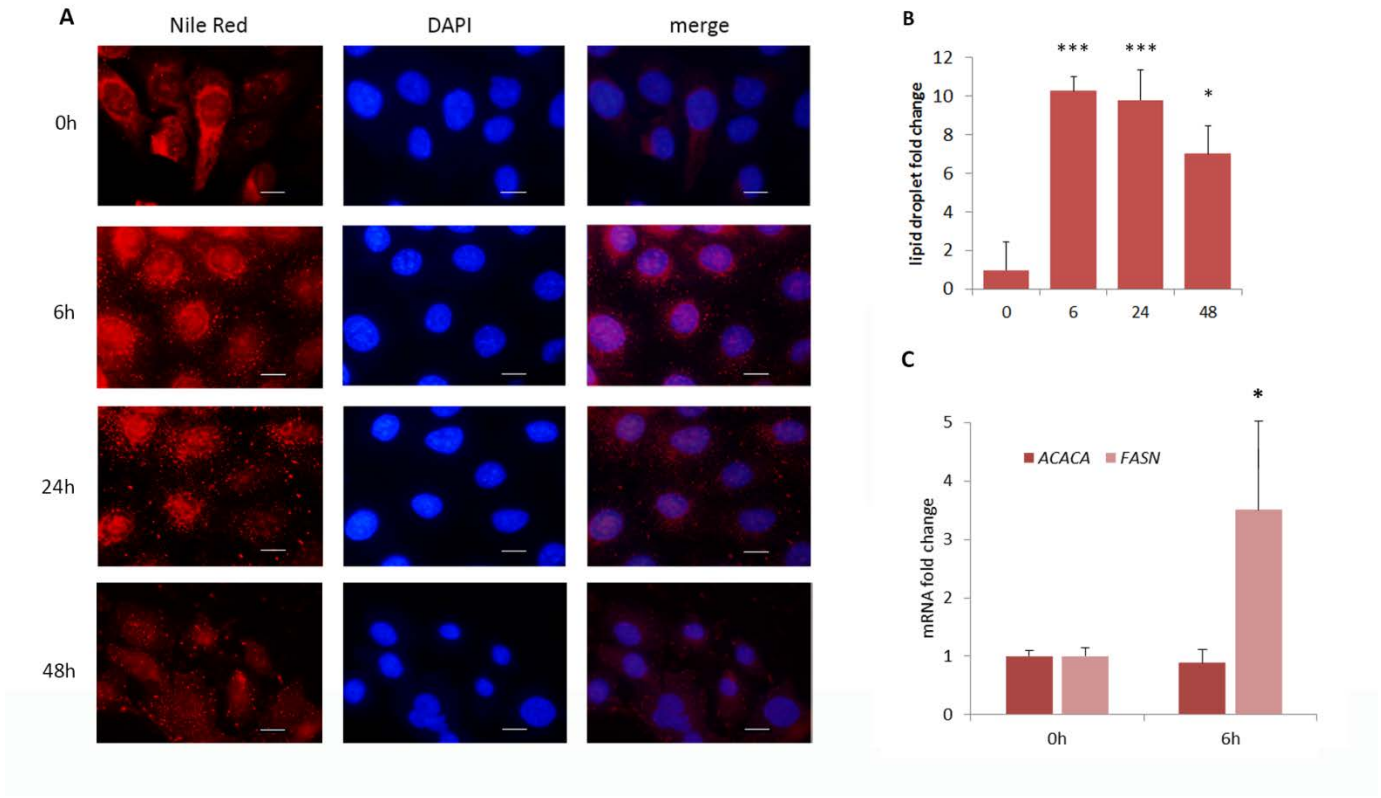


**Figure 4.** Lipid droplets accumulation and mRNA expression of lipogenic enzymes in EMT induced cells. A) Pictures of DU145 cells treated with TNFα (20 ng/ml) for 0, 6 24 and 48 hours and then stained with Nile Red for 20 minutes and DAPI. Representative fluorescence images of the stained cells using red and blue filters are shown. Scale bars: 20 μm. B) Bar diagram of lipid droplets quantification. Results are representative of pictures of three independent experiments. C) Bar diagram of real-time quantitative PCR of ACACA and FASN expression in samples of untreated and 6-hour treated cells with TNFα (20 ng/ml). Results represented the mean ± SE of three independent experiments (n=3) performed in triplicate. * p<0.05, ** p<0.01, *** p<0.005

The untargeted lipidomic approach of the present work was carried out in order to detect changes in specific lipids without any pre-conceived idea about the lipid candidates, which potentially enabled the discovery of novel interesting molecules that could have never been a focus of study in EMT. The main results of this untargeted lipidomic study revealed a significant rise of twelve unsaturated TAG species during the EMT induction in DU145 cells under TNFα treatment. A similar TAG increase was observed under TGFβ exposure, another well-known EMT inducer, suggesting that this common feature could be important for the transition process in epithelial cells. Also, we observed that in EMT induced cells by TNFα and TGFβ, the newly synthesized TAGs accumulated in lipid droplets. TAGs act not only as a reservoir of energy, but also of FAs, which in turn could be used for protein modification, incorporation to other lipid species for cell membrane building and the generation of pro-tumorigenic signals. Thus, this increase of TAG levels could be interpreted as a preparation process of cells for the increasing need for energy, membrane production and signalling lipids essential to guarantee survival and proliferation of metastatic cells.

These results are in agreement with a previous work of Goto et al. on fibrosarcoma cells, in which hypoxia has been shown to upregulate TAG synthesis and to promote the formation of lipid droplets [26]. In addition, pharmacological inhibition of this TAG synthesis has been shown to cancel proliferation and motility of hypoxic cancer cells, indicating that newly synthesized TAGs played an important role in tumour growth and metastasis under hypoxic conditions. Several publications have linked hypoxia and EMT induction[27, 28]. Since in solid tumours most cells exist in chronic hypoxia, TAG synthesis could

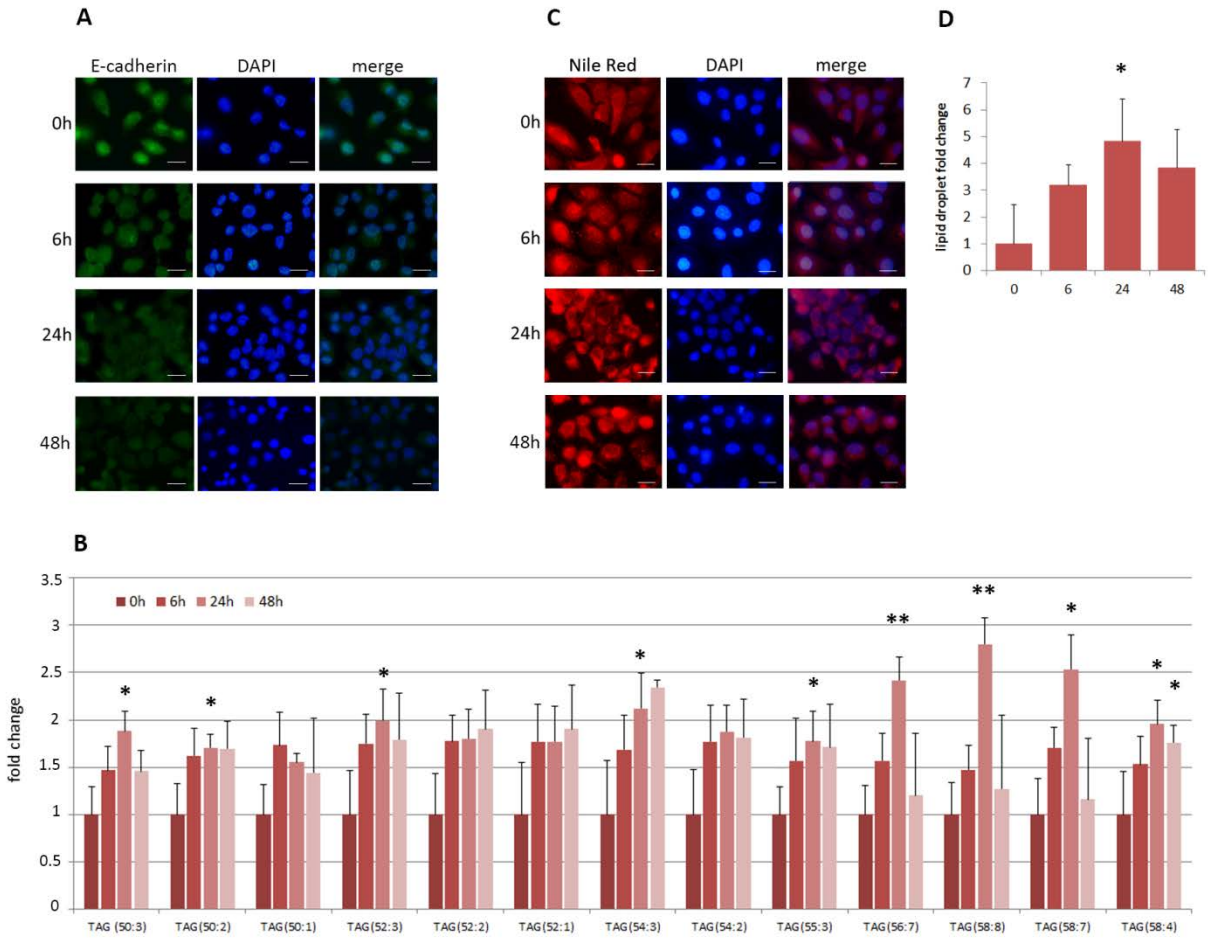


**Figure 5.** EMT induction in DU145 cells using TGFβ. DU145 cells were treated with TGFβ (20 ng/ml) for 0, 6, 24 and 48 hours. A) Immunofluorescence assay of EMT induced cells. After fixation, E-cadherin (green) was examined by green immunofluorescence staining with E-cadherin-FITC antibody. Nuclei were stained with DAPI (blue). Images are representative of several pictures taken in random fields. Scale bars: 20 μm B) Bar diagram of fold changes in the levels of the selected TAGs at the indicated doses. Results are representative of two independent experiments performed in triplicate. The indicated significant differences are considered respect to the untreated cells. C) Pictures of TGFβ treated cells (20 ng/ml) for 0, 6, 24 and 48 hours stained with Nile Red for 20 minutes and DAPI. Representative fluorescence images of the stained cells using red and blue filters are shown. Scale bars: 20 μm D) Bar diagram of lipid droplets quantification. Results are representative of pictures of three independent experiments. * $p<0.05$, ** $p<0.01$

be an interesting subject of study in cancer progression research.

An aberrant increase in de novo lipogenesis has been observed in many cancers [29], including prostate cancer, in which it is significantly associated with tumour progression and worse prognosis [30]. Fatty acid synthase (FASN) which produces palmitate (16:0), has been found to be overexpressed in prostate cancer and to be associated with progression and metastasis [29]. In addition, FASN has been reported to mediate EMT in breast and ovarian cancer cells [31, 32]. In the present study, we also have found a significant increase of FASN under TNFα exposure. This FASN overexpression could be related to the increased TAGs levels, since the newly synthesized FAs are rapidly incorporated into neutral- and phospholipid stores. In contrast to normal cells, these FAs have been reported to account for more than 93% of triacylglycerol FAs in tumour

cells[29]. Although our results suggest that FASN overexpression could be responsible for the rise of TAG in our conditions, the direct involvement of FASN in the TAG synthesis under EMT induction needs to be further investigated.

The generation and accumulation of TAG in metastatic cells has sense if these malignant cells have a complementary lipolytic mechanism able to liberate stored fatty acids for metabolic and signalling needs. This TAG lipolysis is performed through the action of a series of lipases such as hormone-sensitive lipase, adipose triglyceride lipase and monoacylglycerol lipase (MAGL). In this context, the lipolytic enzyme MAGL has been found to be highly elevated in aggressive cells from multiple tissues of origin [33]. This enzyme has demonstrated to generate a wide array of second messenger signals that support migration, survival, and in vivo tumour growth.

Besides the increase of TAGs, our untargeted lipidomic analysis also detected a reduction of Cer (16:0) levels, which is in agreement with the findings of Edmond et al. [18] These authors reported a down-regulation of CerS6 in EMT, the enzyme responsible for its synthesis. They demonstrated that lowered levels of Cer (16:0) enhance membrane fluidity and stimulate cell motility in epithelial tumour cells. In addition to its role in plasma membrane, ceramide is a well-known signalling lipid involved in anti-proliferative responses and apoptosis. According to this, the reduction of ceramide levels observed could be traduced in a decrease of pro-apoptotic signals leading to an enhanced cell survival, necessary for tumour progression.

## Conclusions

The untargeted lipidomic analysis performed in this work revealed a significant increase of twelve unsaturated TAG species in EMT-induced prostate cancer cells. To our knowledge, this feature has never been reported before under EMT induction. This rise of TAGs is concomitant with lipid droplet formation and FASN overexpression, suggesting an activation of the de novo lipogenesis in EMT induced cells. This TAG storage could be explained by an increasing cell need for energy, membrane components and signalling lipids for the enhanced cell migration, proliferation and aggressiveness characteristic of metastatic cells. Since TAGs seem to be the fuel of cancer cells necessary to acquire a malignant phenotype, further research should be addressed to find new therapeutic targets throughout the lipogenic and lipolytic enzymatic pathways that control TAG accumulation.

## Experimental

### Chemicals and reagents

TNFα, TGFβ, cell culture media and reagents were obtained from Sigma. Analytical grade methanol and chloroform were purchased from Merck and Carlo Erba, respectively. HPLC Gradient Grade acetonitrile was from Fischer Chemicals. Lipid standards were obtained from Avanti Polar Lipids.

### Cell culture

The human prostate cancer cell line DU145 was purchased from the American Type Culture Collection and maintained in RPMI1640 culture medium supplemented with 10% heat-inactivated foetal bovine serum, 100 U/ml penicillin and 100 µg/ml streptomycin at 37°C in a humidified atmosphere containing 5% of CO2.

### Immunofluorescence

DU145 cells were seeded in 12-well plates containing glass coverslips at a density of 1.5 x $10^5$cells per well and left in culture until next day. Cells were treated with TNFα (20ng/ml) or TGFβ for 0, 6, 24 and 48hours. Media was aspirated and cells washed with PBS. Cells were fixed with cold methanol for 20 minutes and washed three times with PBS. Next, 20 µl of anti CD324/E-cadherin-FITC was added to each sample. Samples were incubated on ice for one hour, and then washed three times with PBS. Cells were mounted onto glass slides using ProLong® Diamond Antifade Mountant with DAPI (Life Technologies) and left in the dark for 30 minutes, according to the manufacturer's instructions. Samples were examined under a fluorescence microscope (40X, Nikon SMZ 1500, using

DAPI and FTIC filters) fitted with a digital camera (Nikon DS-Ri1).

**Quantitative real-time PCR**

Total mRNA of DU145 cells was extracted after treatment with TNFα for the indicated times (0, 3, 4, 5, 6 hours). Cells were harvested using a rubber scraper into 2 ml of ice-cold PBS. Cells were centrifuged at 1300 rpm for 3 minutes at 4˚C and cell pellets were washed twice with cold PBS. Total RNA was extracted using the NucleoSpin RNA kit (Macherey-Nagel). RNA quality was checked in an Agilent 2100 Bioanalyzer (Agilent Technologies). RNA (2 μg) were retro-transcribed to cDNA using Transcriptor First Strand Synthesis Kit (Roche) and stored at -20˚C. Quantitative PCR analysis was carried out with a LightCycler® 480 Real Time PCR System (Roche) using LightCycler SYBR Green I Master® (Roche). The primers used in each reaction are the following: CDH1 forward 5'-TACACTGCCCAGGAGCCAGA-3' and reverse 5'- TGGCACCA-GTGTCCGGATTA-3'; SNAIL forward 5'- GACCACTATGCCGCG-CTCTT-3' and reverse 5'- GTGGGATGGCTGCCAGC-3'; VIM forward 5'- TGAGTACCGGAGACAGGTGCAG and reverse 5'-TAGCAGCTTCAACGGCAAAGTTC-3'; ACACA forward 5'-CAGAGACTACGTCCTCAAGCAAATC-3' and reverse 5'- CGTAT-GACTTCTGCTCGCTGAGT-3'; FASN forward 5'- GCACCTCTCAG-GCATCGA-3' and reverse 5'- CTGTGGTCCCACTTGATGAG-3'. The gene GAPDH was used as the endogenous control reference gene. The threshold cycle number (Ct value) of different genes was normalized to the Ct value of GAPDH from the same sample, and the fold change in expression was calculated using the ΔΔCt method [34]. Ct values were calculated by technical triplicates.

**Visualization of neutral lipids using Nile Red staining**

DU145 cells were seeded at 5 x $10^4$ cells per well density in 12-well plates containing glass coverslips. Next day, cells were treated with TNFα (20ng/ml) or TGFβ (20ng/ml) for 0, 6, 24 and 48 hours. Next, media was aspirated and cells were fixed for 20 min using cold methanol. Cells were stained for 1 hour by adding 1 ml of a 0.5 mg/L Nile Red (Sigma) solution in acetone. Then, cells were washed with PBS and left in PBS until further use. Finally, coverslips were mounted onto glass slides using ProLong® Diamond Antifade Mountant with DAPI (Life Technologies) and left in the dark for 30 minutes, according to the manufacturer's instructions. Samples were examined under a fluorescence microscope (60X, Nikon SMZ 1500, using DAPI and Red filters) fitted with a digital camera (Nikon DS-Ri1). Quantification of lipid droplets was carried out using ImageJ software on three independent measurements

**Lipid extraction and LC-MS analysis**

DU145 cells were seeded in triplicate in 6-well plates at 2 x $10^5$ cells per well. After 24 hours, cells were treated with TNFα (20ng/ml) for 0, 3, 4, 5 and 6 hours. Cells were harvested using a rubber scraper into 2 ml of ice-cold PBS. Cells were centrifuged at 1300 rpm for 3 minutes at 4˚C and cell pellets were washed twice with cold PBS. Samples were prepared twice to perform two types of lipid extraction: 1) extraction with chloroform/methanol (2:1) that contains intact lipids from the sample; and 2) extraction chloroform/methanol (1:2) with a saponification step that enables the recovery of sphingolipids. For the extraction 1, 100 μl of deionized water were added to the cell pellets and the suspension was transferred to borosilicate glass test tubes with Teflon caps. Then, 250 μl of methanol and 500 μl of chloroform were subsequently added. This mixture was fortified with internal standards of lipids (1,2,3-17:0 triglyceride, 1,3-17:0 D5 diacylgliceride, 17:0 cholesteryl ester, 17:1 lyso phosphatidylethanolamine, 17:1 lyso phosphoglyceride, 17:1 lyso phosphatidylcholine), 200 pmol each (10 μL of 20 μM stock solutions in absolute ethanol). Samples were vortexed and sonicated until they appeared dispersed. Next, the samples were evaporated under N2 stream and transferred to 1.5 ml eppendorf tubes after addition of 500 μl of methanol. Samples were evaporated again and resuspended in 150 μl of methanol. The tubes were centrifuged at 10000 rpm for 3 minutes and 130 μl of the supernatants were transferred to UPLC vials for injection. For the extraction 2, sphingolipids were prepared as described[35]. Briefly, 100 μl of deionized water were added to the cell pellets and the suspension was transferred to borosilicate glass test tubes with Teflon caps. Afterwards, 500 μl of methanol and 250 μl of chloroform were subsequently added. This mixture was fortified with internal

 

standards of sphingolipids (N-dodecanoylsphingosine, N-dodecanoylglucosyl-sphingosine and N-dodecanoylsphingosylphosphorylcholine), 200pmol each (10 μL of 20 μM stock solutions in absolute ethanol). Samples were sonicated until they appeared dispersed, and incubated overnight at 48˚C in a heating water bath. The tubes were cooled and 75 μl of 1M KOH in methanol were added. After 2h incubation at 37°C, KOH was neutralized with 75 μl of 1M acetic acid. The samples were then evaporated under N2 stream and transferred to 1.5 ml eppendorf tubes after addition of 500 μl of methanol. Samples were evaporated again and resuspended in 150 μl of methanol. Finally, the tubes were centrifuged at 10000 rpm for 3 minutes and 130 μl of the supernatants were transferred to UPLC vials for injection.

The LC/MS analysis consisted of a Waters Acquity UPLC system connected to a Waters LCT Premier orthogonal accelerated time of flight mass spectrometer (Waters), operated in both positive and negative electrospray ionization modes. Full scan spectra from 50 to 1500 Da were acquired, and individual spectra were summed to produce data points each of 0.2s. Mass accuracy and reproducibility were maintained by using an independent reference spray via the LockSpray interference. The analytical column was a 100X 2.1-mm inner diameter, 1.7 mm C8 Acquity UPLC bridged ethylene hybrid (Waters). The two mobile phases were phase A: MeOH 1mM ammonium formate and phase B: H2O 2mM ammonium formate. The flow rate was 0.3 ml/min and the gradient of A/B solvents started at 80:20 and changed to 90:2 in 3 min; from 3 to 6 min remained at 90:10; changed to 99:1 in 6 minutes until min 15; remained 99:1 until minute 18; finally returned to the initial conditions until minute 20. Column was held at 30 °C.

**Kinetic study of TAG increase**

DU145 cells were seeded in triplicate in 6-well plates at 2 x $10^5$ cells per well. After 24 hours, cells were treated with TNFα (20ng/ml) for 0, 6, 24 and 48 hours. Cells were harvested using a rubber scraper into 2 ml of ice-cold PBS. Then, cells were centrifuged at 1300 rpm for 3 minutes at 4˚C and cell pellets were washed twice with cold PBS. Lipids were extracted using lipid extraction 1 and analysed using the same system mentioned above. Specific TAG species were integrated using the Masslynx software on the original raw data of samples and areas were further normalized by protein content and the area of the internal TAG standard.

**Chemometric analysis of LC-MS data**

Each UPLC-MS chromatographic run recorded for every sample resulted in a data file which was converted to CDF format by the Databridge program of the MassLynx software. Data was imported into MATLAB environment using mzcdfread and mzcdf2peaks functions from the MATLAB Bioinformatics Toolbox. Working data matrices were built up using in-house functions which bin all values with an m/z resolution of 0.05. This import process generated data matrices containing mass spectra at all retention times in their rows and the chromatograms at all m/z values in their columns. Next, data matrices were normalized taken into account the areas of the internal standards added and the protein content measured for each sample. This normalization was done by multiplying each matrix by a factor obtained as follows: *(200 x mg protein)/mean area of standards*; where 200 refers to the pmol of standards added in the lipid extraction.

These data were analysed in two different steps. First, an exploratory analysis of TICs chromatograms of treated and untreated samples was done by PLS-DA. This step gave us an initial idea about the differences and classification of samples, between pre- and post-EMT (see Supplementary material). Second, a full scan LC-MS data analysis was performed by using MCR-ALS to detect the specific lipids that presented changes under EMT induction and to evaluate the significance of these changes.

In the second data treatment, the detection of specific lipid changes was done using full scan data matrices of every sample only in the positive ionization mode (negative mode samples were not considered as the samples could not be separated in the exploratory PLS-DA models). Due to huge dimensions of these data matrices (e.g. 612 retention times (rows) x 29000 m/z values (columns)), each individual data matrix was subdivided into 11 time windows. These windows

were not equal sized and narrower divisions were made in chromatographic zones where peak signals were more abundant. Every data matrix corresponding to the same time window but to different sample (pre-EMT and post-EMT samples) was then adjoined to a single column-wise augmented data matrix[36-38]. Thus, 11 augmented data matrices were obtained for each type of extraction (a total of 22 matrices). Each augmented matrix was baseline corrected and subsequently scaled using an adaptation of the MinMax algorithm, also known as feature scaling, in order to favour the resolution of lipid profiles present a low concentrations. MinMax algorithm rescales each column of the raw data matrix by subtracting the minimum value to each element of the column and dividing the result by the range of the column. A total of 44 matrices (22 raw and 22 scaled) were subjected separately to MCR-ALS data analysis. This chemometric tool allows the improved mathematical resolution of overlapping multivariate signals of different structure and complexity [39-41]. The successful application of MCR on LC-MS data in –omic studies for the resolution of coeluted and embedded peaks has been recently reported [36-38, 42]. Application of MCR-ALS to the windowed augmented data matrices resulted in the resolution of a number of components, each one represented by a dyad of profiles that described their chromatographic elution and their mass spectra profiles. From the relative areas of these MCR-ALS resolved elution profiles, it is possible to estimate the relative amounts of components in every analysed sample. However, only those components with a significant difference in their elution profile peak areas between pre and post-EMT samples were finally considered for further analysis. Although their MCR-ALS resolved MS spectra profiles at 0.05 m/z resolution may already allow a preliminary identification of the lipid species, a more exact identification is possible using original raw high-resolution data [36, 37, 42]. The corresponding elution peaks at these m/z values were subsequently integrated using the MassLynx software in order to obtain an accurate estimation of the amount of each lipid (identified by its m/z value) in each sample. This is extremely useful in the case of considering normalized data in which each MCR-ALS resolved component could present a relatively high number of candidate m/z values and assignation of MCR-ALS resolved area to a particular peak is not straightforward. The calculated areas were then normalized to concentration of lipids (pmol/mg protein) as follows: (200 x mg of protein)/mean area of standards.

For these normalized concentrations of lipids, fold changes were calculated from the arithmetic mean values of each group. To check whether the difference observed in lipid peak areas between pre- and post-EMT samples were statistically significant, a Mann-Whitney U test was applied considering as a factor the different treatment times. Additionally, a discriminant analysis with PLS-DA was applied to the data matrix containing the concentrations of the selected lipids for each sample (X-data). PLS-DA y-vector had the class labels, pre-EMT (class 0) and post-EMT (class 1) samples for each extraction. These lipid concentration matrices were autoscaled before PLS-DA. Results were cross-validated by the leave-one-out method. Two out of the twenty-four samples analysed were removed appeared as outliers in the Q residuals *vs* $T^2$ plots. The MCC [16] was calculated to validate the goodness of each discrimination model. The MCC is a correlation coefficient between the observed and predicted binary classifications; the returned values are between -1 and +1. A coefficient of +1 indicates a perfect prediction, a value of 0 indicates no better classification than a random prediction and a value of -1 represents total disagreement between prediction and observation. In the PLS-DA model obtained, the VIP scores [17], which estimate the importance of each variable in the projection used in a PLS-DA model, were calculated .

The identification of compounds was only performed for m/z values with statistically significant differences in their areas (p-value of Mann-Whitney U test <0.05). LipidMaps [43] and Human Metabolome Database (HMDB) [44] were used for the identification of lipid species. The assigned compound corresponded to the lipid molecule with the minimum mass error value respect to the measured m/z, considering all the possible adducts in the positive ionization mode. The annotated lipid also had to fulfil an adequate retention time regarding its polarity.

Finally, only identified compounds with a VIP score value greater than 1 and a mass error less than 10 ppm in the lipid

 

identification were selected for a further interpretation of lipidomic results.

**Statistical analysis**

Results are expressed as mean ± SD of three independent experiments unless otherwise specified. To check whether the differences observed in qRT-PCR and kinetic experiments were statistically significant, a Welch's t-test was used. Mann-Whitney U test was used to assess the difference of means between the areas of the identified compounds in the different treatment times. Benjamini-Hochberg procedure has been used to control the false discovery rate.

**Software**

The software used in this work includes MassLynx V 4.1 (Waters) for raw UPLC-TOF data analysis. For matrix data processing and statistical analyses, the Bioinformatics Toolbox (The Mathworks Inc.), PLS-Toolbox (Eigenvector Research Inc.) and MCR-ALS Toolbox [45] were used in MATLAB 8.3.0 – R2013a (The Mathworks Inc.) environment. ImageJ (National Institutes of Health) was used for image processing and analysis.

## Acknowledgements

This work was supported by the European Research Council under the European Union's Seventh Framework Programme (FP/2007-2013)/ERC Grant Agreement 320737. J.J acknowledges a CSIC JAE-Doc contract cofounded by FSE.

## References

1. K. Polyak and R. A. Weinberg, Nature reviews. Cancer, 2009, 9, 265-273.
2. J. P. Thiery and J. P. Sleeman, Nature reviews. Molecular cell biology, 2006, 7, 131-142.
3. J. P. Thiery, H. Acloque, R. Y. Huang and M. A. Nieto, Cell, 2009, 139, 871-890.
4. H. E. Zhau, V. Odero-Marah, H. W. Lue, T. Nomura, R. Wang, G. Chu, Z. R. Liu, B. P. Zhou, W. C. Huang and L. W. Chung, Clinical & experimental metastasis, 2008, 25, 601-610.
5. H. Peinado, D. Olmeda and A. Cano, Nature reviews. Cancer, 2007, 7, 415-428.
6. Y. Wu and B. P. Zhou, Cell cycle, 2009, 8, 3267-3273.
7. V. Michalaki, K. Syrigos, P. Charles and J. Waxman, British journal of cancer, 2004, 90, 2312-2316.
8. M. Kumar, D. F. Allison, N. N. Baranova, J. J. Wamsley, A. J. Katz, S. Bekiranov, D. R. Jones and M. W. Mayo, PloS one, 2013, 8, e68597.
9. G. van Meer, The EMBO journal, 2005, 24, 3159-3165.
10. K. Sandra and P. Sandra, Current opinion in chemical biology, 2013, 17, 847-853.
11. D. Touboul and M. Gaudin, Bioanalysis, 2014, 6, 541-561.
12. P. L. Wood, Neuropsychopharmacology : official publication of the American College of Neuropsychopharmacology, 2014, 39, 24-33.
13. M. Oresic, V. A. Hanninen and A. Vidal-Puig, Trends in biotechnology, 2008, 26, 647-652.
14. R. Guirguis, I. Margulies, G. Taraboletti, E. Schiffmann and L. Liotta, Nature, 1987, 329, 261-263.
15. J. Shankar, A. Messenberg, J. Chan, T. M. Underhill, L. J. Foster and I. R. Nabi, Cancer research, 2010, 70, 3780-3790.
16. B. W. Matthews, Biochimica et biophysica acta, 1975, 405, 442-451.
17. S. Wold, M. Sjöström and L. Eriksson, Chemometrics and Intelligent Laboratory Systems, 2001, 58, 109-130.
18. V. Edmond, F. Dufour, G. Poiroux, K. Shoji, M. Malleter, A. Fouque, S. Tauzin, R. Rimokh, O. Sergent, A. Penna, A. Dupuy, T. Levade, N. Theret, O. Micheau, B. Segui and P. Legembre, Oncogene, 2015, 34, 996-1005.
19. X. Wu, G. Daniels, P. Lee and M. E. Monaco, American journal of clinical and experimental urology, 2014, 2, 111-120.
20. J. Fuxe and M. C. Karlsson, Seminars in cancer biology, 2012, 22, 455-461.
21. C. H. Heldin, M. Vanlandewijck and A. Moustakas, FEBS letters, 2012, 586, 1959-1970.
22. J. Xu, S. Lamouille and R. Derynck, Cell research, 2009, 19, 156-172.
23. M. E. Linder and R. J. Deschenes, Nature reviews. Molecular cell biology, 2007, 8, 74-84.
24. F. Guan, K. Handa and S. I. Hakomori, Proceedings of the National Academy of Sciences of the United States of America, 2009, 106, 7461-7466.
25. F. Guan, L. Schaffer, K. Handa and S. I. Hakomori, FASEB journal : official publication of the Federation of American Societies for Experimental Biology, 2010, 24, 4889-4903.
26. K. Goto, T. Asai, S. Hara, I. Namatame, H. Tomoda, M. Ikemoto and N. Oku, Cancer letters, 2005, 219, 215-222.
27. J. Guo, B. Wang, Z. Fu, J. Wei and W. Lu, Technology in cancer research & treatment, 2015, DOI: 10.1177/1533034614566413.
28. J. V. Joseph, S. Conroy, K. Pavlov, P. Sontakke, T. Tomar, E. Eggens-Meijer, V. Balasubramaniyan, M. Wagemakers, W. F. den Dunnen and F. A. Kruyt, Cancer letters, 2015, 359, 107-116.
29. J. A. Menendez and R. Lupu, Nature reviews. Cancer, 2007, 7, 763-777.
30. G. Zadra, C. Photopoulos and M. Loda, Biochimica et biophysica acta, 2013, 1831, 1518-1532.

31. J. Li, L. Dong, D. Wei, X. Wang, S. Zhang and H. Li, International journal of biological sciences, 2014, 10, 171-180.
32. L. Jiang, H. Wang, J. Li, X. Fang, H. Pan, X. Yuan and P. Zhang, International journal of molecular sciences, 2014, 15, 11539-11554.
33. D. K. Nomura, J. Z. Long, S. Niessen, H. S. Hoover, S. W. Ng and B. F. Cravatt, Cell, 2010, 140, 49-61.
34. K. J. Livak and T. D. Schmittgen, Methods, 2001, 25, 402-408.
35. A. H. Merrill, Jr., M. C. Sullards, J. C. Allegood, S. Kelly and E. Wang, Methods, 2005, 36, 207-224.
36. M. Farrés, B. Piña and R. Tauler, Metabolomics, 2014, DOI: 10.1007/s11306-014-0689-z.
37. E. Gorrochategui, J. Casas, C. Porte, S. Lacorte and R. Tauler, Analytica chimica acta, 2015, 854, 20-33.
38. K. M. G. Lima, C. Bedia and R. Tauler, Microchemical Journal, 2014, 117, 255-261.
39. J. Jaumot, R. Gargallo, A. de Juan and R. Tauler, Chemometrics and Intelligent Laboratory Systems, 2005, 76, 101-110.
40. E. Pere-Trepat, S. Lacorte and R. Tauler, Journal of chromatography. A, 2005, 1096, 111-122.
41. R. Tauler, Chemometrics and Intelligent Laboratory Systems, 1995, 30, 133-146.
42. C. Bedia, N. Dalmau, J. Jaumot and R. Tauler, Environmental research, 2015, 140, 18-31.
43. M. Sud, E. Fahy, D. Cotter, A. Brown, E. A. Dennis, C. K. Glass, A. H. Merrill, Jr., R. C. Murphy, C. R. Raetz, D. W. Russell and S. Subramaniam, Nucleic acids research, 2007, 35, D527-532.
44. D. S. Wishart, T. Jewison, A. C. Guo, M. Wilson, C. Knox, Y. Liu, Y. Djoumbou, R. Mandal, F. Aziat, E. Dong, S. Bouatra, I. Sinelnikov, D. Arndt, J. Xia, P. Liu, F. Yallou, T. Bjorndahl, R. Perez-Pineiro, R. Eisner, F. Allen, V. Neveu, R. Greiner and A. Scalbert, Nucleic acids research, 2013, 41, D801-807.
45. J. Jaumot, A. de Juan and R. Tauler, Chemometrics and Intelligent Laboratory Systems, 2015, 140, 1-12.